Trans-Atlantic correlation of Late Cretaceous high-frequency sea-level cycles

A. Guy Plint[a,b], David Uličný[c,d], Stanislav Čech[e], Ireneusz Walaszczyk[f], Darren R. Gröcke[g], Jiri Laurin[c], Joel A. Shank[a,h], Ian Jarvis[i]

a. Department of Earth Sciences, the University of Western Ontario, London, Ontario, N6A 5B7, Canada. gplint@uwo.ca

b. Corresponding author

c. Institute of Geophysics, Academy of Sciences of the Czech Republic, Boční II/1401, 141 31 Praha 4, Czech Republic.

d. Institute of Geology and Paleontology, Faculty of Science, Charles University, Albertov 6, 128 43 Praha 2, Czech Republic

e. Czech Geological Survey, Klarov 3, 118 21 Praha 1, Czech Republic.

f. Faculty of Geology, University of Warsaw, Al. Żwirki i Wigury 93, PL-02-089 Warszawa, Poland,

g. Department of Earth Sciences, University of Durham, Durham, DH1 3LE, UK.

h. Present address: ExxonMobil Canada East, 100 New Gower St., St. John's, Newfoundland, A1C 6K3, Canada.

i. Department of Geography, Geology and the Environment, Kingston University London, Penrhyn Road, Kingston upon Thames, KT1 2EE, UK

Keywords: Upper Cretaceous, Eustasy, Bohemian Basin, Western Canada Foreland Basin, Sea-Level Change.

ABSTRACT

Previous studies of Cretaceous sedimentary rocks have used multi-proxy correlation methods to suggest eustatic change, modulated by the c. 400 kyr long eccentricity rhythm. Although numerous authors have inferred eustatic changes on shorter timescales, none have demonstrated synchronous sea-level changes in separate basins on different plates, thousands of kilometres apart. Our study integrates basin-scale, three-dimensional sequence architecture, molluscan biostratigraphy, and carbon-isotope chemostratigraphy to demonstrate synchronous sea-level changes in upper Turonian to lower Coniacian shallow-marine clastic successions in the Western Canada Foreland Basin, and the Bohemian Cretaceous Basin. Depositional sequences in both basins are plotted in a common time domain using an astronomically calibrated age model, allowing direct comparison. In both basins, at least seven major transgressive events can be shown to be synchronous within the limits of combined biostratigraphic and chemostratigraphic resolution. 'Major' and 'minor' sequences of late Turonian age appear to have been paced, respectively, by the long (c. 400 kyr) and short (c. 100 kyr) eccentricity cycles. In contrast, early Coniacian sequences evidence pacing by the c. 38 kyr obliquity rhythm. Stratal architecture suggests that sequences developed in response to eustatic changes of c. 14 – 20 m at average rates ranging 0.08 to > 1.3 m/kyr. At a time of 'warm greenhouse' climate, sea-level change of this magnitude and

timescale may not be explicable entirely as a result of thermal- and aquifer-eustasy, and hence glacio-eustasy may also have been a contributing factor.

1. Introduction

Many Cretaceous shallow-marine clastic successions are characterized by transgressive–regressive sequences in which facies changes are suggestive of relative sea-level oscillations of < c. 30 m, commonly on a timescale of < c. 500 kyr. Although the cyclicity has in cases been attributed to tectonic mechanisms (Kamola and Huntoon, 1995), there is increasing acceptance of the idea that many of these high-frequency sequences are of eustatic origin, linked to Milankovitch-band climatic cycles (Gale et al., 2002; Voigt et al., 2006; Laurin and Sageman, 2007; Plint and Kreitner, 2007; Uličný et al., 2014; Lin et al., 2021). Definitive evidence of synchronous sea-level changes between separate basins, especially at < 400 kyr timescale, is still rarely presented (Wilmsen, 2007; Gale et al., 2008). Because of the inferred amplitude and frequency of these sea-level changes, it has been postulated that they could only be attributed to glacio-eustasy (e.g. Miller et al., 2005). This idea is supported by some climate model results (Flögel et al., 2011), and by the presence of Early Cretaceous (Valanginian to Aptian) glacial tills, ice-marginal deposits, and dropstones in the Eromanga Basin of Australia, deposited at a palaeolatitude of between 70 and 80 °S (Alley et al. 2020). The inference of Cretaceous glacio-eustasy is, however, highly controversial in view of faunal, floral, sedimentary, and geochemical evidence that indicate that much of the Cretaceous Period was a greenhouse world, apparently lacking polar ice caps. Recent studies (Hay and Floegel, 2012; Kidder and Worsley, 2012; Sames et al., 2016, 2020; Ray et al., 2019) now emphasize that the Cretaceous climate was not uniformly equable, but oscillated between ‘cool’, ‘warm’ and ‘hot’ greenhouse phases. During warm and hot greenhouse times, polar ice formation, and hence glacio-eustasy, was considered improbable.

A solution to the mechanistic dilemma posed by high-frequency sequences was the proposal of 'aquifer eustasy' (Hay and Leslie, 1990), by which cyclical climate changes caused terrestrial aquifers to alternately fill and drain, resulting, respectively, in sea-level fall, and rise. The amplitude and timescale of aquifer eustasy is, however, subject to wide uncertainty. In their original proposal, Hay and Leslie (1990) estimated that *complete* filling and emptying of terrestrial aquifers might, after isostatic compensation, change sea-level by up to 50 m on a timescale of 10^4 to 10^5 years. In an attempt to explain Milankovitch-band sea-level changes recorded in Triassic rocks, Jacobs and Sahagian (1993) examined the regions of present Earth that were affected by 20 kyr cycles of monsoonal precipitation; they calculated that aquifer-eustasy might contribute from 4 to 8 m of sea-level change, and that similar fluctuations might have driven Triassic sea-level cycles of c. 10 m.

More recently, a series of papers (Wagreich et al. 2014; Sames et al. 2016, Wendler and Wendler, 2016; Wendler et al. 2016, Sames et al. 2020) have emphasized the potential importance of aquifer-eustasy, suggesting that, during the Cretaceous greenhouse (and especially the mid-Cretaceous warm- to hot greenhouse), spatio-temporal shifts in arid and humid zones would have promoted alternate filling and emptying of aquifers in continental interiors, potentially resulting in 50 to perhaps as much as 80 m of eustatic change on a c. 400 kyr timescale, or longer. However, such high-amplitude aquifer eustasy has been challenged by numerical modeling of spatio-temporal variation in the distribution of arid and humid zones for the Valanginian, Turonian, and Maastrichtian (Davies et al. 2020). Model results showed that aquifer-eustasy during these Stages was likely to be in the range of decimetres, and even with extreme forcing, did not exceed 5 m. In a comprehensive review of Phanerozoic eustasy, Simmons et al. (2020) concluded that, for the Cretaceous, a combination of thermo-eustasy and aquifer-eustasy might be able to explain short-term (1.2 Myr or less), eustatic change of c. 10 m, whereas eustatic change in excess of c. 15 m would be unachievable without a contribution from glacio-eustasy.

Any discussion of eustatic mechanisms must be underpinned by tightly constrained stratigraphic evidence for synchronous sea-level changes in widely separated locations, preferably on different plates (Ray et al., 2019). The basis of precise correlation is high-resolution biostratigraphy, but the evidence for synchronous events is strengthened if the stratigraphic architecture of each basin-fill can be established in three dimensions, and if an independent means of correlation, such as chemostratigraphy can be used to support biostratigraphy. Stable carbon-isotope stratigraphy has proven to be an effective high-resolution correlation tool (Jarvis et al., 2006, 2015, 2021; Wendler, 2013; Uličný et al., 2014), and integrated biostratigraphy and carbon-isotope stratigraphy have been used to demonstrate trans-Atlantic correlation of Cenomanian eustatic cycles interpreted to correspond to the 405 kyr long eccentricity cycle (Gale et al., 2008). The new results presented here not only demonstrate synchronous eustatic change on a timescale varying from c. 400 kyr to as little as c. 30 kyr, but also address a stratigraphic interval that commonly is punctuated by numerous hiatuses that can make accurate identification and correlation of sea-level events extremely difficult.

We present the results of a multi-proxy study of shallow marine, siliciclastic strata of late Turonian to early Coniacian age that were deposited about 7000 km apart (Fig. 1). The stratigraphic interval spanning the Turonian–Coniacian (T–C) boundary is well-suited to an inter-basinal study of mid-Cretaceous sea-level change. An important sea-level fall near the T–C boundary has been widely interpreted (Jarvis et al., 2006; Uličný et al., 2014). However, detailed inter-basinal correlation of high-frequency (i.e. << 1 Myr duration) depositional sequences that span the late Turonian to early Coniacian has, in many cases, been prevented by hiatuses such as the Navigation Hardground suite in the classical Chalk sections of the Anglo-Paris Basin, or by regional erosional surfaces that typify many clastic and carbonate sections in other basins (Olszewska-Nejbert, 2004; Jarvis et al., 2006, 2021; Shank and Plint, 2013; Walaszczyk et al., 2014; Gale, 2019).

Although the Western Canada Foreland Basin (WCFB) and Bohemian Cretaceous Basin (BCB) discussed here differ markedly in area (c. 360,000 vs. c. 30,000 km^2 respectively), and in tectonic style (flexural vs. transtensional, respectively), their sedimentary successions preserve evidence of high-frequency depositional cyclicity on a timescale of << 1 Myr. The question of a eustatic control on these sequences is here addressed through detailed correlation, based on a combination of three-dimensional stratigraphic analysis in both basins, molluscan biostratigraphy utilizing species common to both North America and Europe, and organic carbon-isotope stratigraphy. Relatively high biostratigraphic resolution is afforded in the latest Turonian to early Coniacian by a number of closely spaced biostratigraphic markers in both North America and Europe (10 markers in c. 1 Myr, Figs. 2, 3; Walaszczyk et al., 2010, 2014). In addition, because CO_2 is cycled through the ocean–atmosphere system on a timescale of the order of 10^3 yr (Siegenthaler and Sarmiento, 1993), carbon-isotope stratigraphy potentially affords a comparable, <10 kyr degree of temporal resolution. In this study, the chronostratigraphic timescale that serves as the basis for correlation is derived from the reference $\delta^{13}C$ time series of the Bch-1 core (BCB; Uličný et al., 2014). This dataset represents, to date, the highest temporal resolution among published Upper Turonian–Coniacian $\delta^{13}C$ curves.

2. Materials and methods

2.1 Correlation methods

Regional stratigraphy in both the WCFB and BCB was established through the correlation of transgressive–regressive depositional sequences, bounded by marine flooding surfaces, using grids of hundreds to thousands of wireline logs, supplemented by core and outcrop data (Plint et al., 1986; Hart and Plint, 1993; Laurin and Uličný, 2004, Uličný et al., 2009, 2014; Shank, 2012; Shank and Plint, 2013). Macrofossils in outcrop and core were integrated into the three-dimensional physical stratigraphic framework, which included sections sampled for carbon isotope analysis (Walaszczyk et al., 2014). In the BCB, this included a continuous core in the Bch-1 research well, used as a new reference section for the middle to upper Turonian and for the T–C boundary (Uličný et al., 2014). A time-domain portrayal of the carbon-isotope curve from Bch-1 (Fig. 2), spanning the upper Turonian to lower Coniacian interval, provides a common chronostratigraphic framework for trans-Atlantic correlation, based on a new astrochronological timescale (Laurin et al., 2014, 2015). Age estimates in Ma given in the present paper are based on this model and include error margins as specified in Jarvis et al. (2015). The most tightly constrained correlation between the two basins has been established between the LO (Lowest Occurrence) of *Prionocyclus germari* (Reuss) and the LO of *Cremnoceramus crassus crassus* (Petrascheck), spanning ~ 700 kyr (Laurin et al., 2014; Figs. 2, 3). In order to provide a broader chemostratigraphic context for the high-resolution correlations across the T–-C boundary, a correlation of the entire Upper Turonian is here proposed.

2.2. Stratigraphic data: Cardium Formation, Western Canada Foreland Basin

The Cardium Formation is a clastic, shallow-marine to alluvial unit, up to ~150 m thick, that was deposited on a broad, low-gradient, NE-facing ramp that spanned the proximal (western) foredeep of the WCFB. Abundant, publicly-accessible wireline logs and cores have provided the data for an allostratigraphic subdivision of the formation, based primarily on the correlation of marine transgressive or flooding surfaces (Plint et al., 1986). Such an approach has allowed the internal architecture of the formation to be determined in detail, and on a basin scale (Fig. 4).

The Cardium Formation comprises a stack of regionally mappable, disconformity-bounded, sandier-upward successions, interpreted to comprise transgressive, highstand and falling-stage deposits. Lowstand deposits are bounded below by unconformable ‘E’ surfaces and above by transgressive ‘T’ surfaces. Lowstand units are typically conglomeratic, lenticular in dip view, and form metres-thick, strike-elongate bodies isolated on the outer part of the ramp. To seaward and landward of the lowstand deposits, the bounding ‘E’ and ‘T’ surfaces merge into composite disconformities, labelled E1 through E7 (Plint et al., 1986; Plint, 1988; Hart and Plint, 1993; Shank and Plint, 2013; Figs. 3, 4). Transgressive surfaces are mantled by cm- to dm-thick veneers of extra-basinal pebbles that were reworked landward from lowstand shoreface deposits. Collectively, each of the upward-shoaling successions, plus the overlying conglomeratic cap, is interpreted as a depositional sequence that records a full cycle of relative sea-level change. Nine principal sequences have now been mapped within the formation in Alberta and British Columbia. The nine sequences are organized into three major progradational packages, the lower between surfaces E1 and E4, the middle between surfaces E4 and E5, and the upper between surfaces E5 and E7 (Shank and Plint, 2013; Figs. 3, 4).

Sequence stacking in the Cardium Formation becomes increasingly progradational between surfaces E1 and E5, accompanied by an increasingly tabular stratal geometry, both features being interpreted to indicate a gradual decrease in flexural subsidence rate (Shank, 2012; Shank and Plint, 2013). Two thin, latest

Turonian sequences between E5 and E5.5 are sheet-like, onlap landward onto E5 and indicate the onset of sea-level rise but no increase in subsidence rate. Slow subsidence prevailed in the earliest Coniacian, resulting in condensation or non-deposition between E5.5 and E6. Foredeep subsidence accelerated markedly following E6 time, resulting in a dramatic westward thickening of the interval between E6 and E7 (Shank and Plint, 2013; Figs. 3, 4).

A relatively expanded, shore-proximal section through the Cardium Formation, fully exposed on the Bow River at Horseshoe Dam, Alberta (51° 07´ 04.45˝ N 115° 02´ 11.45˝ W; Fig. S1), was chosen for detailed sequence- and biostratigraphic study (Shank and Plint, 2013; Walaszczyk et al., 2014; Fig. 3). The entire succession at Horseshoe Dam was sampled at 0.5 m intervals for carbon isotopes, and a supplementary section at Ghost River (51° 16´ 15.39˝ N 114° 55´ 09.23˝ W; Figs. 3, S1), was also sampled, with sample spacing ranging from 1 m to as little as 0.2 m in the vicinity of the Turonian–Coniacian boundary to better characterize the isotopic changes across that interval. Additional data, in particular the LO of *C. deformis erectus*, and an auxiliary C-isotope curve, based on samples with 0.5 m spacing, were obtained from a distal basin succession at Deer Creek (Montana). Wireline logs allowed the Deer Creek section to be correlated to Horseshoe Dam (Fig. S2; Shank and Plint, 2013; Walaszczyk et al., 2014).

2.3. Stratigraphic data: Jizera and Teplice Formations, Bohemian Cretaceous Basin,

Czech Republic

In the BCB, the Cardium Formation has temporal equivalents in the Jizera and Teplice formations (Čech and Uličný, 2021, and references therein). These clastic units were deposited in nearshore deltaic, shoreface, and offshore to hemipelagic environments in several fault-bounded sub-basins within a major, reactivated intra-continental fault zone (Voigt et al., 2008). The correlations presented here focus on the northwestern sub-basin of the BCB where the genetic sequence stratigraphy and detailed biostratigraphy of the sandstone-dominated deltaic wedges are best documented (Uličný et al., 2009). The Český Ráj depocentre is of particular importance because the T–C boundary is preserved there in a well-exposed succession of coarse-grained deltas (Čech and Uličný, 2021).

The Jizera Formation (Figs. 3, 5) in the central BCB region is dominated by strongly bioturbated, mixed siltstones and marlstones that indicate deposition in offshore to hemipelagic environments that grade landward into distal prodelta to lower shoreface environments. Relative to the location of the Bch-1 core hole, the nearest shoreline lay about 35 km to the NW (Uličný et al., 2014). In the regional genetic-stratigraphic scheme based on maximum transgressive surfaces (Uličný et al., 2009), the Jizera Formation of the Český Ráj depocentre comprises genetic sequences TUR 5 through 6/1 (Fig. 5), with the base of TUR 6/1 much less pronounced than in the type area of the western BCB (Laurin and Uličný, 2004). This part of the study interval was generally characterized by relatively high sedimentation rates (c. 20 cm/kyr) in a hemipelagic realm and preserves a conspicuous cyclic signal in elemental proxy parameters such as the Si/Al ratio (Fig. 3). Fluctuations in this ratio are interpreted as a record of precession cycles modulated by short eccentricity, that governed the input of coarser grained clastics into the basin (Fig. S4; Chroustová et al., 2021).

The highest upper Turonian and lower Coniacian strata in the Český Ráj depocentre comprise sandstone-dominated, Gilbert-type deltas that prograded generally southward from the faulted basin margin, into water as much as c. 100 m deep. The deltaic clinothems pass downdip into heterolithic, turbidite-dominated bottomset facies, and further basinward into offshore mudstone and marlstone of the Teplice Formation (Laurin and Uličný, 2004; Uličný et al., 2009, 2014; Čech and Uličný, 2021). A number of deltaic sandstone wedges are grouped into a single package, the Hrubá Skála Sandstone Member of the Teplice Formation, that shows a forestepping geometry of thick, deep-water delta bodies in the lower part, overlain by a much thinner package of backstepping shallow-water delta bodies, in turn capped by offshore marly mudstone (Fig. 5). The Hrubá Skála Sandstone and its distal correlatives correspond to sequences TUR 7 and CON 1 defined in the western part of the basin (Uličný et al., 2009). Within the Hrubá Skála Sandstone, individual prograding deltaic clinothems, separated by minor transgressive surfaces, were labelled HS-1 through HS-8 by Čech and Uličný (2021). The shift from a long-term progradational to a retrogradational stacking pattern occurs between HS-6 and HS-7 (Fig. 5).

Genetic sequences TUR 5 and TUR 6/1 in the BCB form a long-term progradational succession that overlies a major, basinwide transgressive surface and is terminated above by a flooding surface that marks the lowest occurrence of the ammonite *Prionocyclus germari*. Sequence TUR 6/2 contains the first steeply-dipping, sand-dominated clinothems belonging to the Hrubá Skála Sandstone, but as a whole TUR 6/2 shows a relative backstep and is separated from the younger TUR 7 sequence by another major transgressive surface. The subsequent long-term progradation of deltaic units HS-2 to HS-6 is interrupted by a transgressive event at the LO of *Cremnoceramus waltersdorfensis waltersdorfensis* (Andert). The change from progradation to retrogradation at the base of local sequence HS-7 coincides with the LO of *Cremnoceramus crassus inconstans* (Woods). The final drowning of the entire Hrubá Skála deltaic system coincides with the base of the *C. crassus crassus* Zone (base of CON 2 sequence; Čech and Uličný, 2021). Despite the tectonic activity at the adjacent basin margin and differential subsidence in the depocentre (Fig. 5), the above transgressive surfaces are correlated widely, interpreted as basinwide and most likely of eustatic origin.

Three significant regressive intervals, attributed to relative sea-level falls, stand out in the BCB: (1) the terminal lowstand of sequence TUR 5; (2) long-distance progradation of HS-2 (= TUR 7 elsewhere in the basin); (3) marked progradation of small-scale sequences HS-4 and HS-5 associated with offlap within the CON 1 sequence (Čech and Uličný, 2021).

2.4. Analytical methods.

The carbon-isotope data presented here (Figs. 2, 3) are based on: (i) previously published datasets of $\delta^{13}C_{org}$ and $\delta^{13}C_{carb}$ from the Bch-1 core in the BCB (Uličný et al., 2014; Jarvis et al., 2015); (ii) a new suite of $\delta^{13}C_{org}$ analyses of samples from Alberta and Montana. Analytical work was undertaken at the Stable Isotope Biogeochemistry Laboratory (SIBL) at the University of Durham. Sedimentary samples were ground to a fine powder (ca. 10 µm) using a Retsch agate mortar grinder RM100. The bulk rock powders (ca. 5 mL) were decalcified using 3 M HCl overnight at room temperature (20 °C) in 50 mL centrifuge tubes. Insoluble residues were rinsed three to four times with deionized water, subsequently dried at 50 °C, reground in an agate mortar, and stored in glass vials until isotopic analysis could be performed.

Organic carbon isotope ($\delta^{13}C_{org}$) measurements were performed on 2.5–3 mg splits of the insoluble residues using a Costech elemental analyser (ESC 4010) connected to a Thermo Scientific Delta V Advantage isotope ratio mass spectrometer via a Conflo III interface. Carbon isotope ratios are reported in standard delta (δ) notation in per mil (‰) relative to VPDB. Data accuracy was monitored through analyses of international and in-house standards calibrated against the international standards (viz., IAEA-CH-3, IAEA-CH-6, IAEA-CH-7, IAEA-N-1, IAEA-N-2, NBS 24, USGS40). Analytical uncertainty for carbon isotope measurements was ±0.1‰ for replicate analyses of standards and <0.2‰ on replicate sample analyses.

2.5 Assessment of subsidence and sea-level change

In the Cardium Formation, the E3 to E7 interval provides the best opportunity to estimate the magnitude of eustatic change, based on stratal offlap and onlap patterns, and from a determination of the pattern of subsidence. Shank (2012) showed, on the basis of isopach mapping, that regional flexural tectonic subsidence rate decelerated from E1 to E3, became low to negligible between E3 and E6, but then accelerated markedly between E6 and E7. For the E3 to E6 interval, isopach maps showed that subsidence was primarily due to the isostatic effect of a 'slab load' of sediment and water. In order to make simple estimates of subsidence based on isopach maps, Airy isostasy was assumed; shallowly buried, semi-compacted sediment density was assumed to be 2.3 g/cm^3, asthenospheric mantle = 3.4 g/cm^3 and water = 1 g/cm^3. The observed thickness of mixed mudstone-sandstone lithologies was decompacted to a nominal 'shallow burial depth' by expansion by 30%. Supplementary Data provides more detailed discussion of estimates of sea-level change in the Cardium Formation.

For the BCB, estimated subsidence rates during the Turonian and Coniacian were published by Uličný et al. (2009) and the reader is referred to the Appendix in that paper for the decompaction procedure applied.

3. Results

3.1 Inter-basinal correlation

The Canadian and Bohemian basins were characterized by temporally and spatially non-uniform rates of subsidence that complicate comparison of sequence stacking patterns. In the WCFB, the nearshore succession close to the T–C boundary is punctuated by hiatuses, whereas in the BCB the stage boundary interval is recorded in both nearshore and offshore facies (Figs. 2–5). Correlations can nevertheless be established because of the availability of high-resolution biostratigraphic and carbon-isotope data, coupled with the chronostratigraphic age model, that allow the succession of depositional sequences to be compared between basins (Laurin et al., 2014, 2015; Fig. 2). Importantly, the successions of inoceramid bivalves in the Canadian and Bohemian basins are essentially identical (Walaszcyk et al., 2014; Čech and Uličný, 2021), and the lowest occurrences of key taxa appear to be synchronous within the resolution of the $\delta^{13}C$ chronostratigraphy.

The most marked difference between the two datasets is in the long-term sequence stacking patterns. In particular, the timing of maximum offlap in the T–C interval differs significantly between the WCFB and BCB. The interval represented by the E5 surface in the WCFB occurs in the latest Turonian and appears to span 89.9 – 90.1 Ma (Fig. 6). In the BCB, the main hiatus is in the early Coniacian, with maximum offlap at c. 89.6 Ma (Fig. 6). This discrepancy is the result of differences in the timing of tectonic events – temporary cessation of flexural subsidence in the WCFB vs. accelerated subsidence in the north-eastern BCB (Shank and Plint, 2013; Čech and Uličný, 2021). In datasets of lower stratigraphic resolution, these two unconformities could easily be misinterpreted as the same "eustatic" event.

Viewed at a higher stratigraphic resolution, four major transgressive events coincide, respectively, with the LOs of *P. germari*, *C. waltersdorfensis waltersdorfensis, C. crassus inconstans* and *C. crassus crassus*. The LO of *C. w. waltersdorfensis* was not identified at Horseshoe Dam, but can be correlated from other sections to a level immediately above the T5.5 surface (Walaszczyk et al., 2014). This correlation is further supported by the marked minimum in $\delta^{13}C_{org}$ in the Ghost River section, interpreted as a record of part of the Navigation carbon-isotope event (CIE) (Fig. 3). In addition to the above four flooding surfaces, three other surfaces are less well constrained biostratigraphically, but are correlated on the basis of $\delta^{13}C$ trends: (1) the basinwide flooding at base of the TUR 5 sequence in the BCB appears to correlate to the E1a surface in the WCFB; (2) an unnamed but marked transgressive surface early in TUR 5, at the level of the Bridgewick CIE in the BCB, correlates to the E2 surface in the WCSB; and (3) the flooding surface at the base of TUR 6/1 (Laurin & Uličný, 2004) overlies a short-term lowstand recognized elsewhere in Central Europe (Čech and Uličný, 2021), and matches a similarly pronounced $\delta^{13}C$ trend across the E4 surface in the WCFB (Fig. 3).

Whereas the LO of *P. germari* is associated with marked flooding events in both regions, the subsequent transgression associated with the *Didymotis* Event "0" in the BCB and the base of TUR 7 sequence, is not recognizable at Horseshoe Dam: either a coeval transgressive event did not occur there or, more probably, equivalent strata below the E5 surface are only preserved in the distal, subsurface part of the basin (Figs. 3, 6).

In addition to the foregoing seven transgressive events, here considered synchronous within the resolution of the bio- and $\delta^{13}C$ stratigraphy, prominent lowstand events also correlate between the BCB and WCFB. At least three high-frequency pulses of sea-level rise followed the E4 lowstand in the WCFB (Pattison and Walker, 1992), and these events are correlated to the TUR 5 lowstand–transgressive interval in the BCB, spanning 4–5 precession cycles (Figs. 2, 6). The prominent offlapping to lowstand package (Keith, 1991; Fraser, 2012; Fic, 2013) between surfaces E4 and E5 in the WCFB (Fig. 4) is correlative with the long-distance regression recorded by the TUR 7 sequence in the BCB (Fig. 5; Uličný et al., 2009; Nádaskay and Uličný, 2014). A falling stage to lowstand phase is interpreted in the BCB to represent local sequences HS-4 through HS-6 in the *C.w. hannovrensis* Zone of the Hrubá Skála Sandstone (Čech and Uličný, 2021) and may correlate to the E5.7 and E6 surfaces.

4. Sea-level changes

4.1. Timescale of sea-level change

A tentative, qualitative sea-level curve (Fig. 6) is based on the correlation of principal transgressive and regressive events between the two study areas. Comparison of the relative sea level histories to the Bch-1 age model reveals an apparent change in the timing of the main transgressive and regressive events within the studied interval. This change involves sea-level cycles, on at least two timescales, both operating over < 1 Myr. Genetic sequences TUR 5 and 6/1 together represent c. 864 kyr in the Bch-1 age model, and sequence TUR 6/2 represents c. 382 kyr. The duration estimates and patterns of cyclicity suggest control by the c. 400-kyr eccentricity modulation of the precession rhythm. This is supported by the spectral estimate for the

Si/Al siliciclastic proxy that follows the transgressive–regressive pattern of genetic sequences TUR5 through TUR7 and suggests an elevated power in the 400-kyr band (Fig. S4).

In younger strata, the relative sea-level cycles appear to be of higher frequency. Within TUR 7 sequence lasting c. 246 kyr, four short-term genetic sequences are recognized (Čech and Uličný, 2021), giving an estimated duration of a short-term sequence of c. 61 kyr. In the CON 1 sequence that lasted c. 243 kyr, six short-term regressive pulses recognized by Čech and Uličný (2021) in HS 3-8 have, on average, a duration of 40.5 kyr, whereas the correlative interval in the WCFB, between surfaces E5.5 and E7, contains four principal sequences with an average duration of 67.5 kyr. Both estimates are well below the 100 kyr eccentricity cycle; at least in the BCB, the short-term cyclicity estimate is closest to the axial obliquity cycle (c. 38 kyr in the Cretaceous; Laskar et al., 2004).

Simplistic estimates such as these need to be treated with caution, however. In the BCB, the total number of local sequences is based on an incompletely preserved record of the Hrubá Skála deltaic complex. Potential additional, unrecorded sequences would further shorten the estimated cycle duration; at the same time, some sequences may have recorded episodes of delta lobe switching, superimposed on longer-term relative sea-level trends. The correlation of high-frequency sequences appears to be closest in the *C. c. inconstans* Zone that lasted about 60 kyr (Laurin et al., 2014): in both basins, this Zone contains two principal accommodation cycles (Fig. 3). The potential relationship of these sea-level cycles to either precessional or obliquity forcing is unclear.

4.2. Amplitude and rate of sea-level change

The amplitude of eustatic change in both the WCSB and BCB has been estimated on the basis of mapped regional stratal geometry and thickness, calibrated against absolute age derived from isotopic data and an age model (Fig. 6). These data allow net subsidence rate to be estimated for each stratal package. An appreciation of subsidence rate is a prerequisite to any attempt to determine eustatic change. Details of the method by which eustatic change was estimated are given in Supplementary Data.

In the WCFB, eustatic fall below E4 (Fig. 6) and subsequent transgression above E4 is estimated to have been about 14 m, with an average rate of change estimated at c. 0.28 m/kyr. The E4.5 to E5 interval was a time of negligible flexural subsidence. It is characterized by the offlap of at least 20 small sequences below E5, which is then overlain by two onlapping wedges comprising the E5 to E5.2 and E5.2 to E5.5 sequences. The observed offlap and onlap geometries below and above E5 indicate net eustatic fall and subsequent rise of c. 20 m, implying an average rate of eustatic change of c. 0.08 m/kyr for each half cycle. The E5.5 to E6 package also records negligible flexural subsidence, and facies offset across E5.5 suggests eustatic rise of at least 15 m, with comparable fall across E6, at a rate of c. 0.2 m/kyr. The E6 to E7 interval was characterized by renewed rapid flexural subsidence, at about 1.3 m/kyr, and comprises two sequences, each spanning ~ 30 kyr. Relative sea-level fall events at E6.5 and E7 imply that the rate of eustatic fall must have twice exceeded c. 1.3 m/kyr.

In the BCB, eustatic fall is inferred to have matched or exceeded subsidence rate during TUR 7 regression (equivalent to E5 to E5.5 package), at an average rate of c. 0.2 – 0.3 m/kyr (Uličný et al., 2009). The relative sea-level rise that drowned the TUR 7 package (HS-2) in the latest Turonian involved at least 13 m of eustatic component (comparable to 15 m at equivalent E5.5 surface in Alberta) at a rate of c. 0.5 m/kyr. Thus, evidence from both study areas suggests that Late Turonian sea-level fell in the range of 14 – 20 m at rates of 0.08 to 0.28 m/kyr, whereas in the Early Coniacian, the frequency of eustatic change appears to have been higher, involving excursions of 15 m or more, at rates in the range 0.5 to 1.3 m/kyr.

5. Discussion

Although synchronous short-term sea-level changes on a timescale of as little as 30 kyr are indicated by our data, their causal mechanisms remain difficult to determine. It is widely acknowledged that short-term (< 1 Myr) Cretaceous eustatic changes are controlled by orbitally driven climate cycles that can change sea-level through three mechanisms: (1) the upper limits of thermal-eustasy (maximum of 10 m) and (2) glacio-eustasy (c. 200 m) are well-known, whereas estimates of (3) aquifer-eustasy are very variable, ranging from 4 to 100 m (Ray et al., 2019).

The relative importance of glacio- and aquifer-eustasy is considered to vary between cool, warm and hot greenhouse climate phases. Some have argued that the

Turonian was an ice-free 'warm greenhouse' where only thermal- and aquifer-eustasy were responsible for short-term eustatic change (Ladant and Donnadieu, 2016; O'Brien et al., 2017; Sames et al., 2016, 2020). Aquifer-eustasy is driven by expanding and contracting humid and arid climate zones. Arid regions have the greatest potential to store and release groundwater because aquifers in humid regions are always nearly full. This mechanism has been estimated to operate on a timescale of 10^4 to 10^5 years, and to yield c. 10 – 50 m of eustatic change (Hay and Leslie, 1990; Sames et al., 2016). This conclusion was challenged by Davies et al. (2020) who modeled the climatic forcing effect of varying atmospheric CO_2 on the areal extent of arid zones. Their study suggested that aquifer-eustasy in the Turonian would be < 2 m.

Ray et al. (2019) pointed out that increased global temperature should, according to the aquifer-eustasy concept of Wendler and Wendler (2016), produce the highest humidity and most effective groundwater recharge, and consequently the largest eustatic response. Broad-based estimates of eustatic change through the Cretaceous showed, however, that the peak greenhouse (Albian to Coniacian) was also characterized by the lowest amplitude of eustatic change (c. 30 m). This reasoning led Ray et al. (2019) to conclude that glacio-eustasy must have played some part in controlling sea-level, even at peak greenhouse.

As shown in Figure 6, the most prominent transgressive events in the study interval coincide with marked negative $\delta^{13}C$ intervals (the Bridgewick and Navigation CIEs; $\delta^{13}C$ trough on top of the Hitch Wood 2 CIE). This observation may provide support for an aquifer-eustatic mechanism which, as shown by Laurin et al. (2019), could have resulted in coupling between the global hydrological and carbon cycles. Storage of organic matter on land in lakes and environments of high water-table would coincide with charged aquifers and lower sea levels and increased $\delta^{13}C$ values – and vice versa. The covariance between the inferred sea level curve and $\delta^{13}C$ values (Fig. 6) is, however, far from universal.

The Cardium Formation may provide evidence for co-variance between sea-level and hydrological changes over the Rocky Mountain Cordillera. Extra-basinal conglomerate is present mainly in lowstand shoreface deposits, whereas highstand and falling-stage deposits are dominated by sandstone. This observation may provide independent evidence for a linkage between sea-level fall and higher river discharge that triggered a short-lived advance of the gravel front in rivers, allowing pebbles to reach the lowstand shoreline. Eustatic fall of the estimated c.10 – 20 m would, alone, be inadequate to steepen river gradients across a coastal plain at least 100 km wide, sufficient to initiate gravel supply to the coast (Plint et al., 2018).

Although there appears to be an increase in the frequency of short-term sea-level cycles near the T–C boundary, from eccentricity-dominated to obliquity-dominated, this inference requires further testing with expanded data sets having improved stratigraphic resolution. Our observations, nonetheless, suggest that the interpreted rates and amplitudes of late Turonian and early Coniacian eustatic change, and associated pulses of molluscan evolution, could have been superimposed on either a secular trend, or a singular change in the climate system that led to a shift towards higher-frequency and higher-rate sea-level changes in the Coniacian. The evidence for c. 14 – 20 m of short-term eustatic change, at rates ranging from 0.08 to 1.3 m/kyr, may imply control by a combination of aquifer- and glacio-eustasy, supplemented by a minor thermo-eustatic component (cf. Simmons et al. 2020). Our estimates of eustatic change are smaller than the c. 50 m maximum range inferred on the basis of the stratal stacking pattern in Middle Turonian to Lower Coniacian strata in New Mexico (Lin et al., 2021). Although the << 1 Myr timescale of change in both studies is comparable, direct correlation of results is precluded by the lack of a carbon-isotope or biostratigraphic framework in the study of Lin et al. (2021).

6. Conclusions

1. In upper Turonian to lower Coniacian strata, at least seven major transgressive events documented in the WCFB and the BCB are shown to be synchronous within the limits of biostratigraphic and stable C-isotope resolution, implying a eustatic control. Eustatic changes are estimated to have been in the range 14 – 20 m, and possibly more. Inferred average rates of sea-level change range from 0.08 to > 1.3 m/kyr.

2. The timing of major flooding and lowstand events, based on the available age model, suggests that sea-level changes during the late Turonian took place on a timescale close to the 400- and 100-kyr eccentricity cycles. In contrast, early Coniacian sequences in the BCB, and, in part, those in the WCFB, appear to have been paced by the obliquity rhythm.

3. The succession of high-frequency sea-level changes identified here explains why the T–C boundary interval, worldwide, is marked by one or more hiatuses. The exact timing of major offlap episodes, however, depended on tectonic processes in individual basins, and the amalgamation of several short-term hiatuses, and/or poor stratigraphic resolution could lead to incorrect age assignment of unconformities and of sea-level histories.

4. It is not possible to provide definitive evidence for or against a glacio-eustatic mechanism acting in this time interval. Glacio-eustasy, driven by Milankovitch-band climatic cycles, is proven to provide the necessary amplitude and frequency necessary to explain our observations. If the conclusions of Simmons et al. (2020) are accepted, then our interpreted eustatic changes of 14 to 20 m suggest some component of glacio-eustasy. Although the timescale and potential amplitude of aquifer-eustasy is less well-understood, it is nevertheless also a plausible contributor to Cretaceous eustatic change, and the correlation of major flooding events to lowered $\delta^{13}C$ values supports the operation of this mechanism in at least part of the record.

Acknowledgements

AGP acknowledges funding, spanning several grant cycles, of his research on Western Canada Cretaceous stratigraphy, by the Natural Sciences and Engineering Research Council of Canada (NSERC). He thanks Neil Landman for identifying *Scaphites patulus* from Horseshoe Dam. We thank S. Galić, M. Grifi, R. Langham and T. Plint for their assistance in the field. DU, SČ and JL were supported by the Czech Science

Foundation (GAČR), grant No. 17-10982S, and by the Czech Academy of Sciences through Programme 67985530. SČ acknowledges long-term support by the Czech Geological Survey. Field and laboratory assistance by M. Vopat and A. Uličný is appreciated. DG and IJ were funded by UK Natural Environment Research Council (NERC) grants NE/H021868/1 and NE/H020756/1. IW was supported by the Polish National Science Centre (NCN) Grant no. 2018/31/B/ST10/01820. JAS acknowledges an NSERC postgraduate scholarship. We thank two anonymous referees for their reviews of the manuscript.

Author contributions

The initial concept of the paper was developed jointly by AGP and DU in 2004, and subsequently elaborated with input from DG and IJ in 2010. In Canada, AGP and JAS undertook stratigraphic analysis and isotopic sampling, and IW conducted biostratigraphic analysis. In the Czech Republic, DU and SČ undertook stratigraphic analysis and isotopic sampling, SČ conducted biostratigraphic analysis, and JL constructed the age model and evaluated astronomical signatures in elemental proxy data. DG conducted carbon-isotope analyses on the WCFB samples. All authors contributed to interpretation of data.

Competing financial interests

The authors declare no competing financial interests.

References

Alley, N.F., Hore, S.B., Frakes, L.A., 2020. Glaciations at high-latitude Southern Australia during the Early Cretaceous. Australian J. Earth Sci. 67, 1045–1095.

Čech, S., Uličný, D., 2021. The Turonian–Coniacian stage boundary in an expanded siliciclastic succession: integrated stratigraphy in deltaic through offshore facies, Bohemian Cretaceous Basin. Cret. Res.117, 104576 https://doi.org/10.1016/j.cretres.2020.104576.

Chroustová, M., Holcová, K., Laurin, J., Uličný, D., Hradecká, L., Hrnková, M., Čech, S., Hrouda, F., Jarvis, I., 2021 Response of foraminiferal assemblages to precession-paced environmental variation in a mid-latitude seaway: Late Turonian greenhouse of Central Europe. Marine Micropal. 167, 102025 https://doi.org/10.1016/j.marmicro.2021.102025.

Davies, A., Gréselle, B., Hunter, S.J., Baines, G., Robson, C., Haywood, A.M., Ray, D.C., Simmons, M.D., van Buchem, F.S.P., 2020. Assessing the impact of aquifer-eustasy on short-term Cretaceous sea-level. Cret. Res. 112, 104445 https://doi.org/10.1016/j.cretres.2020.104445.

Fic, J.D., 2013. Characterization of the lower shoreface to offshore reservoir facies of the Cardium Formation in East Pembina, Alberta. M.Sc. thesis, University of Calgary, 128 p.

Flögel, S., Wallmann, K., Kuhnt, W., 2011. Cool episodes in the Cretaceous – Exploring the effects of physical forcings on Antarctic snow accumulation. Earth Planet. Sci.

Lett. 307, 279–288.

Fraser, J.A., 2012. High resolution sequence stratigraphy and reservoir characterization of shoreline deposits of the Cardium Formation at West Pembina, Alberta. M.Sc. thesis, University of Calgary, 89 p.

Gale, A., 2019. Correlation, age and significance of Turonian Chalk hardgrounds in southern England and northern France: The roles of tectonics, eustasy, erosion and condensation. Cret. Res. 103, 104164 https://doi.org/10.1016/j.cretres.2019.06.010.

Gale, A.S., Hardenbol, J., Hathway, B., Kennedy, W.J., Young, J.R., Phansalkar, V., 2002. Global correlation of Cenomanian (Upper Cretaceous) sequences: Evidence for Milankovitch control on sea level. Geology 30, 291–294.

Gale, A.S., Voigt, S. Sageman, B.B., Kennedy, W.J., 2008. Eustatic sea-level record for the Cenomanian (Late Cretaceous) – Extension to the Western Interior Basin, USA. Geology 36, 859–862.

Hart, B.S. Plint, A.G., 1993. Origin of an erosion surface in shoreface sandstones of the Kakwa Member (Upper Cretaceous Cardium Formation, Alberta): Importance for reconstruction of stratal geometry and depositional history. In: Posamentier, H.W., Summerhayes, C.P., Haq, B.U., Allen, G.P. (Eds.), Sequence Stratigraphy and Facies Associations. Int. Assoc. Sedimentol. Spec. Pub. 18, Blackwell Science, Oxford, 451–467.

Hay, W.W., Leslie, M.A., 1990. Could possible changes in global ground water reservoir cause eustatic sea-level fluctuations? In: Revelle, R. (Ed.), Sea Level Change. Nat. Res. Council, Studies in Geophys. Washington D.C. Nat. Acad. Press, 161–170.

Hay, W.W., Flögel, S., 2012. New thoughts about Cretaceous climate and oceans. Earth-Sci. Rev. 115, 262–272.

Jacobs, D.K., Sahagian, D.L., 1993. Climate-induced fluctuations in sea level during non-glacial times. Nature 361, 710–712.

Jarvis. I., Gale, A.S., Jenkyns, H.C., Pearce, M.A., 2006. Secular variation in Late Cretaceous carbon isotopes: a new $\delta^{13}C$ carbonate reference curve for the Cenomanian–Campanian (99.6–70.6 Ma). Geol. Mag. 143, 561–608.

Jarvis, I., Trabucho-Alexandre, J., Gröcke, D.R., Uličný, D., Laurin, J., 2015. Intercontinental correlation of organic carbon and carbonate stable isotope records: evidence of climate and sea-level change during the Turonian (Cretaceous). Dep. Record 1, 53–90.

Jarvis, I., Pearce, M., Püttmann, T., Voigt, S., Walaszczyk, I., 2021. Palynology and calcareous nannofossil biostratigraphy of the Turonian – Coniacian boundary: the proposed boundary stratotype at Salzgitter-Salder, Germany and its correlation in NW Europe. Cret. Res. 123, 104782 https://doi.org/10.1016/j.cretres.2021.104782

Joo, Y.J., Sageman, B.S., 2014. Cenomanian to Campanian isotope chemostratigraphy from the Western Interior Basin, U.S.A. J. Sedim. Res. 84, 529–542.

Kamola, D.L., Huntoon, J.E., 1995. Repetitive stratal patterns in a foreland basin sandstone and their possible tectonic significance. Geology 23, 177–180.

Keith, D.A.W., 1991. Truncated prograding strandplain or offshore sand body? – sedimentology and geometry of the Cardium (Turonian) sandstone and conglomerate at Willesden Green field, Alberta. In: Swift, D.J.P., Oertel, G.F., Tillman, R.W., Thorne, J.A., (Eds.), Shelf sand and sandstone bodies, geometry, facies and sequence stratigraphy. Int. Assoc. Sedimentol. Spec. Pub. 14, Blackwell Science, Oxford, 457–487.

Kidder, D.L., Worsley, T.R., 2012. A human-induced hothouse climate? GSA Today 22, 4–11.

Ladant, J.-B., Donnadieu, Y., 2016. Palaeogeographic regulation of glacial events during the Cretaceous supergreenhouse. Nature Comm. 7, 12771https://doi.org/10.1038/ncomms12771.

Laskar, J., Robutel, P., Joutel, F., Gastineau, M., Correia, A.C.M., Levrard, B., 2004. A long-term numerical solution for the insolation quantities of the Earth. Astron. Astrophys. 428, 261–285 https://doi.org/10.1051/0004-6361:20041335.

Laurin, J., Uličný, D., 2004. Controls on a shallow-water hemipelagic carbonate system adjacent to a siliciclastic margin: Example from Late Turonian of central Europe. J. Sedim. Res. 74, 697–717.

Laurin, J., Sageman, B.B, 2007. Cenomanian–Turonian coastal record in SW Utah, U.S.A.: Orbital-scale transgressive-regressive events during oceanic anoxic event II. J. Sedim. Res. 77, 731–756.

Laurin, J., Čech, S., Uličný, D., Štaffen, Z., Svobodová, M., 2014. Astrochronology of the Late Turonian: implications for the behavior of the carbon cycle at the demise of peak greenhouse. Earth Planet. Sci. Lett. 394, 254–269.

Laurin, J., Meyers, S.R., Uličný, D., Jarvis, I., Sageman, B.B., 2015. Axial obliquity control on the greenhouse carbon budget through middle- to high-latitude reservoirs. Paleoceanography 30, 133–149.

Laurin, J., Barclay, R.S., Sageman, B.B., Dawson, R.R., Pagani, M., Schmitz, M., Eaton, J., McInerney, F.A., McElwain, J.C., 2019. Terrestrial and marginal-marine records of the mid-Cretaceous Oceanic Anoxic Event 2 (OAE 2): High-resolution framework, carbon isotopes, CO_2 and sea-level change. Palaeogeog. Palaeoclimatol. Palaeoecol. 542, 118–136.

Lin, W., Bhattacharya, J.P., Jicha, B.R., Singer, B.S., Matthews, W., 2021. Has Earth ever been ice-free? Implications for glacio-eustasy in the Cretaceous greenhouse age using high-resolution sequence stratigraphy. Geol. Soc. Am. Bull. 133, 243–252.

Miller, K.G., Wright, J.D., Browning, J.V., 2005. Visions of ice sheets in a greenhouse world. Mar. Geol. 217, 215–231.

Nádaskay, R., Uličný, D., 2014. Genetic stratigraphy of Coniacian deltaic deposits of the northwestern part of the Bohemian Cretaceous Basin. Z. Dt. Ges. Geowiss. 165, 547–575.

O'Brien, C.L. and 26 others, 2017. Cretaceous sea-surface temperature evolution: Constraints from TEX_{86} and planktonic foraminiferal oxygen isotopes. Earth-Sci. Rev. 172, 224–247.

Olszewska-Nejbert, D., 2004. Development of the Turonian/Coniacian hardground boundary in the Cracow Swell area (Wielkanoc quarry, southern Poland). Geol. Quart. 48, 159–170.

Pattison, S.A.J., Walker, R.G., 1992 Deposition and interpretation of long, narrow sandbodies underlain by a basinwide erosion surface: Cardium Formation, Cretaceous Western Interior Seaway, Alberta, Canada. J. Sedim. Petrol. 62, 292–309.

Plint, A.G., 1988. Sharp-based shoreface sequences and "offshore bars" in the Cardium Formation: Their relationship to relative changes in sea level. In: Wilgus, C.K., Hastings, B.S., Posamentier, H.W., van Wagoner, Ross, C.A., Kendall, C.G. St.C., (Eds.), Sea Level Changes: An Integrated Approach. Soc. Econ. Paleontol. Miner., Spec. Pub. 42, 357–370.

Plint, A.G., Kreitner, M.A., 2007. Extensive, thin sequences spanning Cretaceous foredeep suggest high-frequency eustatic control: Late Cenomanian, Western Canada foreland basin. Geology 35, 735–738.

Plint, A.G., Walker, R.G., Bergman, K.M., 1986. Cardium Formation 6. Stratigraphic framework of the Cardium in subsurface. Bull. Can. Petrol. Geol. 34, 213–225.

Plint, A.G., Krawetz, J.R., Buckley, R.A., Vannelli, K.M., Walaszczyk, I., 2018. Tectonic, eustatic and climatic controls on marginal marine sedimentation across a flexural depocentre: Paddy Member of Peace River Formation (Late Albian), Western Canada Foreland Basin. Deposit. Record 4, 4–58.

Ray, D.C., van Buchem, F.S.P., Baines, G., Davies, A., Gréselle, B., Simmons, M.D., Robson, B., 2019. The magnitude and cause of short-term eustatic Cretaceous sea-level change: A synthesis. Earth-Sci. Rev. 197, 102901 https://doi.org/10.1016/j.earscirev.2019.102901

Sames, B., Wagreich, M., Wendler, J.E., Haq, B.U., Conrad, C.P., Melinte-Dobrinescu, M.C., Hu, X., Wendler, I., Wolfgring, E., Yilmaz, I.Ö., Zorina, S.O., 2016. Review: Short-term sea-level changes in a greenhouse world - A view from the Cretaceous. Palaeogeog. Palaeoclimatol. Palaeoecol. 441, 393–411.

Sames, B., Wagreich, M., Conrad, C.P., Iqbal, S., 2020. Aquifer-eustasy as the main driver of short-term sea-level fluctuations during Cretaceous hothouse climate phases. In: Wagreich, M., Hart, M.B., Sames, B., Yilmaz, I. (Eds.), Cretaceous climate events and short-term sea-level changes. Geol. Soc. London, Spec. Pub. 498, 9–38 https://doi.org/10.1144/SP498-2019-105.

Shank, J.A., 2012. Sedimentology and allostratigraphy of the Cardium Formation (Turonian–Coniacian) in southern Alberta and equivalent strata in northern Montana. PhD thesis, Univ. Western Ontario, 374 p.

Shank, J.A., Plint, A.G., 2013. Allostratigraphy of the Upper Cretaceous Cardium Formation in subsurface and outcrop in southern Alberta, and correlation to equivalent strata in northwestern Montana, Bull. Can. Petrol. Geol. 61, 1–40.

Siegenthaler, U., Sarmiento, J.L., 1993. Atmospheric carbon dioxide and the ocean. Nature 365, 119–125.

Simmons, M.D., Miller, K.G., Ray, D.C., Davies, A., van Buchem, F.S.P., Gréselle, B.,

2020. Phanerozoic eustasy. In: Gradstein, F.M., Ogg, J.M. Schmitz, M.D., Ogg, G.M. (Eds.), A Geologic Time Scale, Chapter 13, Elsevier, Amsterdam, 357–400.

Uličný, D. Laurin, J., Čech, S., 2009. Controls on clastic sequence geometries in a shallow-marine transtensional basin: the Bohemian Cretaceous Basin, Czech Republic. Sedimentology 56, 1077–1114.

Uličný, D., Jarvis, I., Gröcke, D.R., Cech, S., Laurin, J., Olde, K., Trabucho-Alexandre, J., Švábenická, L., Pedentchouk, N., 2014. A high-resolution carbon-isotope record of the Turonian stage correlated to a siliciclastic basin fill: Implications for mid-Cretaceous sea-level change. Palaeogeog. Palaeoclimatol. Palaeoecol. 405, 42–58.

Voigt, S., Gale, A.S., Voigt, T., 2006. Sea-level change, carbon cycling and palaeoclimate during the Late Cenomanian of northwest Europe: an integrated palaeoenvironmental analysis. Cret. Res. 27, 836–858.

Voigt, S., Wagreich, M.., Surlyk, F., Walaszczyk, I., Uličný, D. Čech, S., Voigt, T., Wiese, F., Wilmsen, M., Niebuhr, B., Reich, M., Funk, H., Michalík, J., Jagt., J.W.M., Felder, P.J., Schulp A.S., 2008. Cretaceous. In: Geology of Central Europe, Volume 2: Mesozoic and Cenozoic (ed. by T. McCann), 923–997. The Geological Society, London.

Wagreich, M., Lein, R., Sames, B., 2014. Eustasy, its controlling factors, and the limno-eustatic hypothesis – concepts inspired by Eduard Suess. Austrian J. Earth Sci. 107, 115–131.

Walaszczyk. I., Wood, C.J., Lees, J.A., Peryt, D., Voigt, S., Wiese, F., 2010. The Salzgitter-Salder quarry (Lower Saxony, Germany) and Słupia Nadbrzeżna river cliff section (central Poland): a proposed candidate composite Global Boundary Stratotype Section and Point for the base of the Coniacian Stage (Upper Cretaceous). Acta Geol. Pol. 60, 445–477.

Walaszczyk, I., Shank, J.A., Plint, A.G., Cobban, W.A., 2014. Inter-regional correlation of disconformities in Upper Cretaceous strata, Western Interior Seaway: Biostratigraphic and sequence-stratigraphic evidence for eustatic change. Geol. Soc. Am. Bull. 126, 307–316.

Wendler, I., 2013. A critical evaluation of carbon isotope stratigraphy and biostratigraphic implications for Late Cretaceous global correlation. Earth-Sci. Rev. 126, 116–146.

Wendler, J.E., Wendler, I., 2016. What drove sea-level fluctuations during the mid-Cretaceous greenhouse climate? Palaeogeog. Palaeoclimatol. Palaeoecol. 441: 412–419.

Wendler, J.E., Wendler, I., Vogt, C., Kuss, J., 2016. Link between cyclic eustatic sea-level change and continental weathering: Evidence for aquifer-eustasy in the Cretaceous. Palaeogeog. Palaeoclimatol. Palaeoecol. 441, 430–437.

Wilmsen, M., 2007. Integrated stratigraphy of the upper Lower – lower Middle Cenomanian of northern Germany and southern England. Acta Geol. Pol. 57, 263–279.

Figure Captions

Fig. 1. Turonian palaeogeographic map of the Earth (after R. Blakey, cpgeosystems.com) showing the location of the two study areas.

Fig. 2. Bio-, chemo-, and chronostratigraphic framework of this study. Shown are the Bohemian and WCFB carbon-isotope records (Bch-1 core, both $\delta^{13}C_{carb}$ and $\delta^{13}C_{org}$; Horseshoe Dam, $\delta^{13}C_{org}$) along with the Chalk $\delta^{13}C_{carb}$ reference curve (Jarvis et al., 2006) and the Colorado composite $\delta^{13}C_{org}$ record (Joo and Sageman, 2014). All data plotted in the time domain using the age model of Laurin et al. (2015). Interpreted positions of named carbon-isotope events and their abbreviations follow Uličný et al. (2014) and Jarvis et al. (2015). Hiatuses in the Western Canadian succession follow nomenclature of key surfaces in the WCFB explained in text. T4 –T6 and Co1 – labelled CIEs in the Colorado composite curve from Joo and Sageman (2014). LO – lowest occurrence of index macrofossil.

Fig. 3. Comparison of lithological, C-isotope records, and biostratigraphic tie points between the sections in Alberta and Bohemia. The Si/Al ratio in the Bch-1 section has been used as a supplementary criterion for interpreting the transgressive-regressive history. In part of the Upper Turonian, the astrochronological interpretation of the Si/Al data (after Laurin in Chroustová et al., 2021) helped to estimate the timescale of lithological cyclicity in Bohemia, and of the E3 and E4 hiatuses in Alberta. "~100 kyr" =

inferred short-eccentricity signal (Gaussian filter, 0.035 ±0.02 cycles/m); "~20 kyr" = inferred precessional signal (Gaussian filter, 0.21 ±0.06 cycles/m; Chroustová et al., 2021). Diagenetic silicification has altered the primary record in the topmost part of the Si/Al record in Bch- 1.

Fig. 4. Summary dip section through the Cardium alloformation, modified after Shank and Plint (2013). Allomembers are defined by regionally-mapped composite ‘E/T’ (erosion/transgression) surfaces that record sea-level fall and subaerial or submarine erosion, followed by transgressive erosion and reworking. E and T surfaces define the lower and upper boundaries of conglomeratic lowstand shoreface deposits, but merge into composite surfaces to landward and seaward. Note that surface ‘E5.7’ is present in the Horseshoe Dam area but has not been mapped regionally, as have the other surfaces. In the original scheme of Plint et al. (1986) the Kakawa ‘allomember’, comprising a shoreface sandstone, was defined (erroneously) on partially lithostratigraphic grounds, and hence letters (N), (B) and (H) are appended to denote temporal equivalence of shoreface sandstone facies to time-equivalent offshore facies of the Nosehill, Bickerdike and Hornbeck allomembers. Thin tongues of coastal plain facies underlie the E5, E6 and E7 surfaces in the far western part of the basin. The coastal plain facies of the Musreau allomember include muddy floodplain and lagoonal mudstones, and small-scale channel-filling sandstone bodies, but no palaeovalleys are known on any bounding surface.

Fig. 5. Schematic, along-dip correlation panel of showing sedimentary units in NE Bohemia, across the Turonian–Coniacian boundary (modified after Čech and Uličný, 2021). Horizontal scale is approximate due to projection of some sections into the correlation line (see map in Fig. S.3), and to the SE of section 28, a great distance to the Bch-1 reference core. Datum varies due to changes of depositional geometry in time and space: to the NW of section 5, correlation is hung on top of sequence HS 2, between sections 4 and 25 on top of sequences HS 7 and HS 6.

Fig. 6. Simplified chronostratigraphic (Wheeler) diagrams based on cross-sections of the study interval in both WCFB and BCB, correlated using the Bch-1 $\delta^{13}C_{org}$ record and biostratigraphic datums plotted in the time domain (based on age model of Laurin et al., 2015). Abbreviations: *Ccc - Cremnoceramus crassus crassus; Cci - C. crassus inconstans; Cde, C. def. erectus - C. deformis erectus; Cww - C. waltersdorfensis waltersdorfensis; Cwh - C. waltersdorfensis hannovrensis, Mh – Mytiloides herbichi.* Hyph. Ev. - Hyphantoceras Event assemblage. Filtered signal of 400 kyr-scale cyclicity shown is derived from Si/Al data in Bch-1 (see Fig. 3, S4 and text for details). Derivation of the eustatic curve and estimated magnitudes of eustatic change for selected cycles are explained in text.

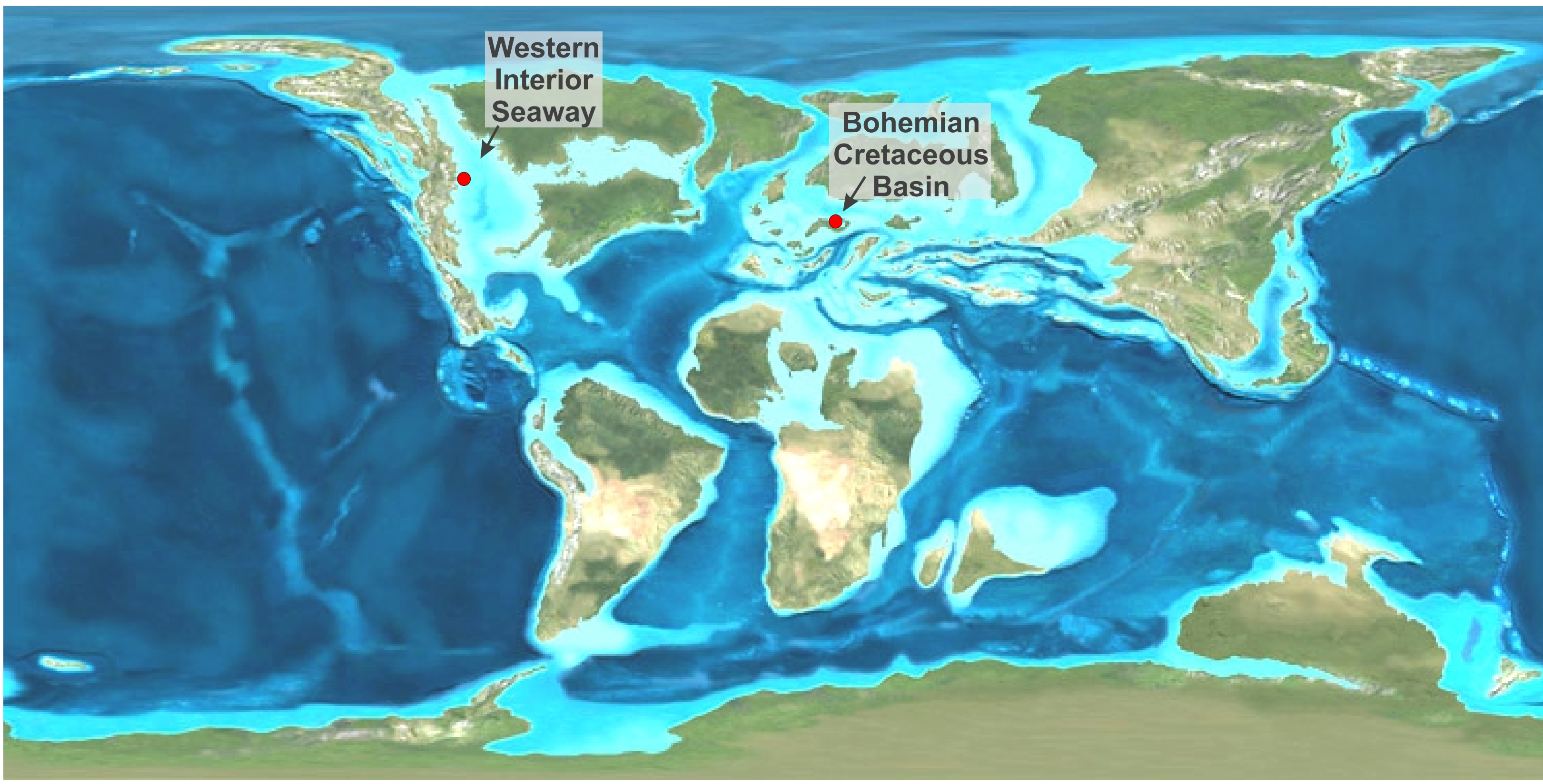
Western Interior Seaway
Bohemian Cretaceous Basin

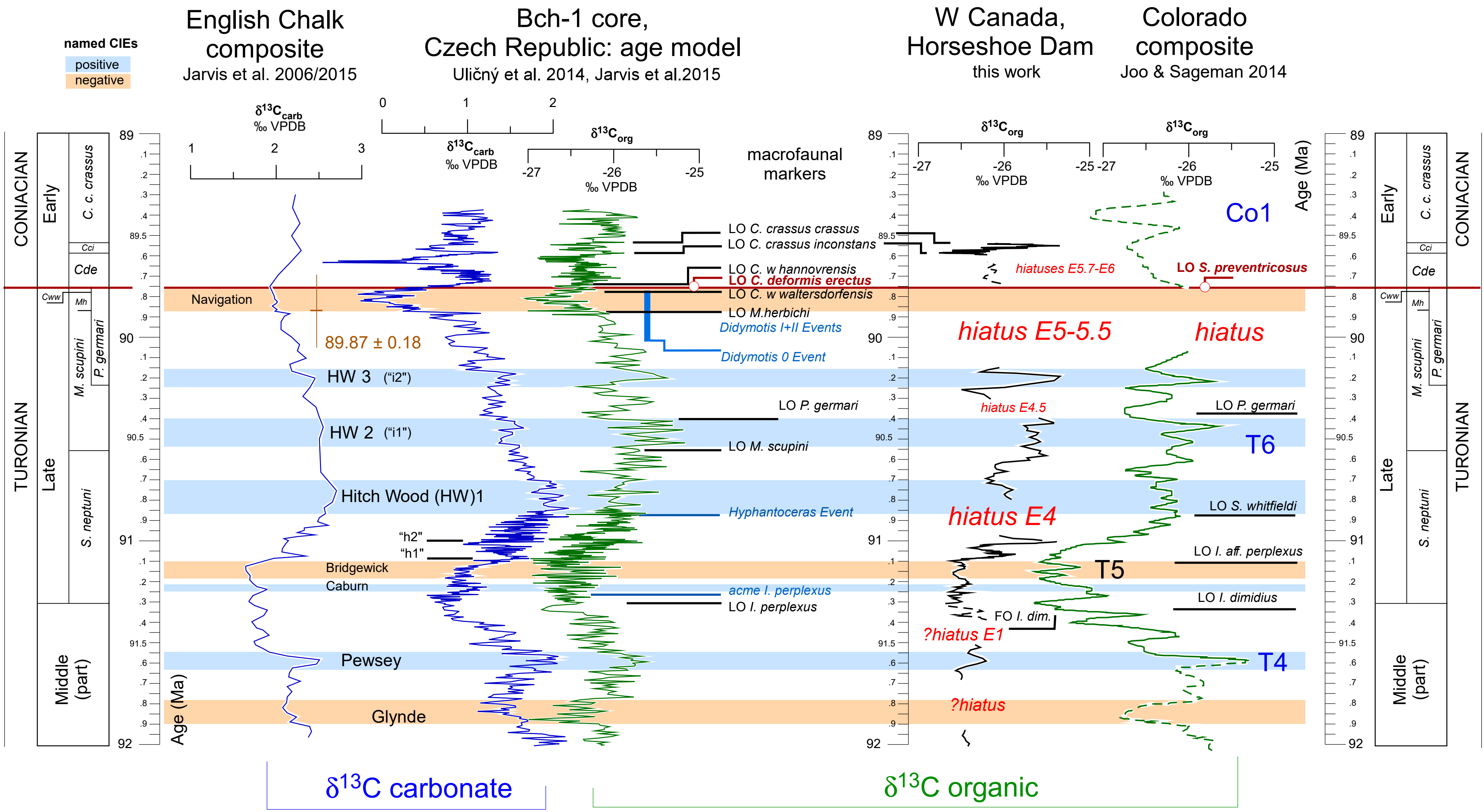

named CIEs
positive
negative
English Chalk composite
Jarvis et al. 2006/2015
Bch-1 core, Czech Republic: age model
Uličný et al. 2014, Jarvis et al.2015
W Canada, Horseshoe Dam
this work
Colorado composite
Joo & Sageman 2014
δ13Ccarb ‰ VPDB
δ13Corg ‰ VPDB
macrofaunal markers
Age (Ma)
CONIACIAN
TURONIAN
Early
Late
Middle (part)
C. c. crassus
Cci
Cde
Cww
Mh
M. scupini
P. germari
S. neptuni
Navigation
89.87 ± 0.18
HW 3 ("i2")
HW 2 ("i1")
Hitch Wood (HW)1
"h2"
"h1"
Bridgewick
Caburn
Pewsey
Glynde
LO C. crassus crassus
LO C. crassus inconstans
LO C. w hannovrensis
LO C. deformis erectus
LO C. w waltersdorfensis
LO M.herbichi
Didymotis I+II Events
Didymotis 0 Event
LO P. germari
LO M. scupini
Hyphantoceras Event
acme I. perplexus
LO I. perplexus
hiatuses E5.7-E6
hiatus E5-5.5
hiatus E4.5
hiatus E4
FO I. dim.
?hiatus E1
?hiatus
LO S. preventricosus
hiatus
Co1
T6
T5
T4
LO P. germari
LO S. whitfieldi
LO I. aff. perplexus
LO I. dimidius
δ13C carbonate
δ13C organic

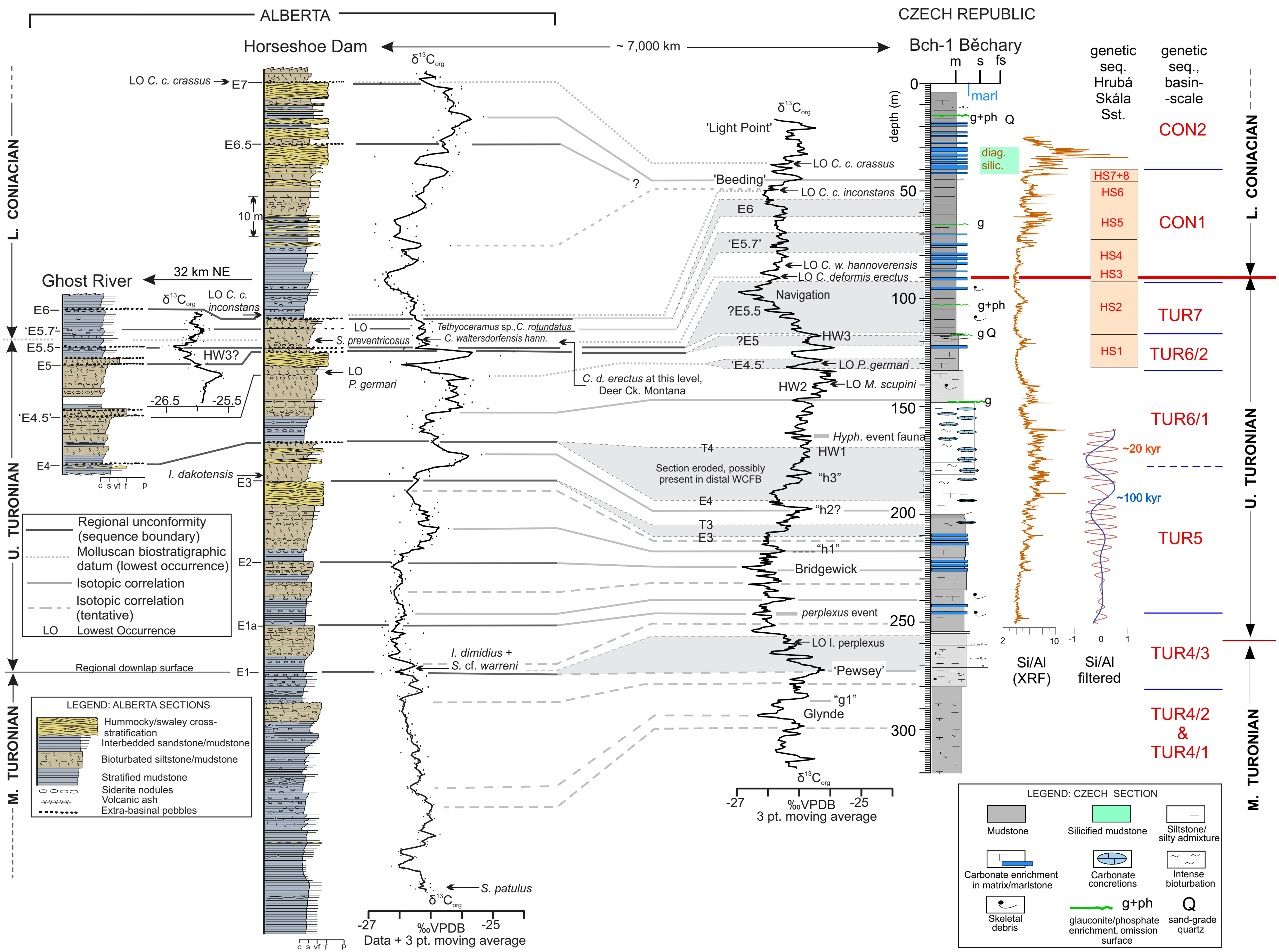

ALBERTA
CZECH REPUBLIC
Horseshoe Dam
~ 7,000 km
Bch-1 Běchary
Ghost River
32 km NE
L. CONIACIAN
U. TURONIAN
M. TURONIAN
genetic seq. Hrubá Skála Sst.
genetic seq., basin-scale
CON2
CON1
TUR7
TUR6/2
TUR6/1
TUR5
TUR4/3
TUR4/2 & TUR4/1
HS7+8
HS6
HS5
HS4
HS3
HS2
HS1
'Light Point'
'Beeding'
Navigation
HW3
HW2
HW1
Bridgewick
'Pewsey'
Glynde
Section eroded, possibly present in distal WCFB
Regional downlap surface
Regional unconformity (sequence boundary)
Molluscan biostratigraphic datum (lowest occurrence)
Isotopic correlation
Isotopic correlation (tentative)
LO Lowest Occurrence
LEGEND: ALBERTA SECTIONS
Hummocky/swaley cross-stratification
Interbedded sandstone/mudstone
Bioturbated siltstone/mudstone
Stratified mudstone
Siderite nodules
Volcanic ash
Extra-basinal pebbles
LEGEND: CZECH SECTION
Mudstone
Silicified mudstone
Siltstone/ silty admixture
Carbonate enrichment in matrix/marlstone
Carbonate concretions
Intense bioturbation
Skeletal debris
glauconite/phosphate enrichment, omission surface
sand-grade quartz
Si/Al (XRF)
Si/Al filtered
~20 kyr
~100 kyr
‰VPDB
Data + 3 pt. moving average
3 pt. moving average

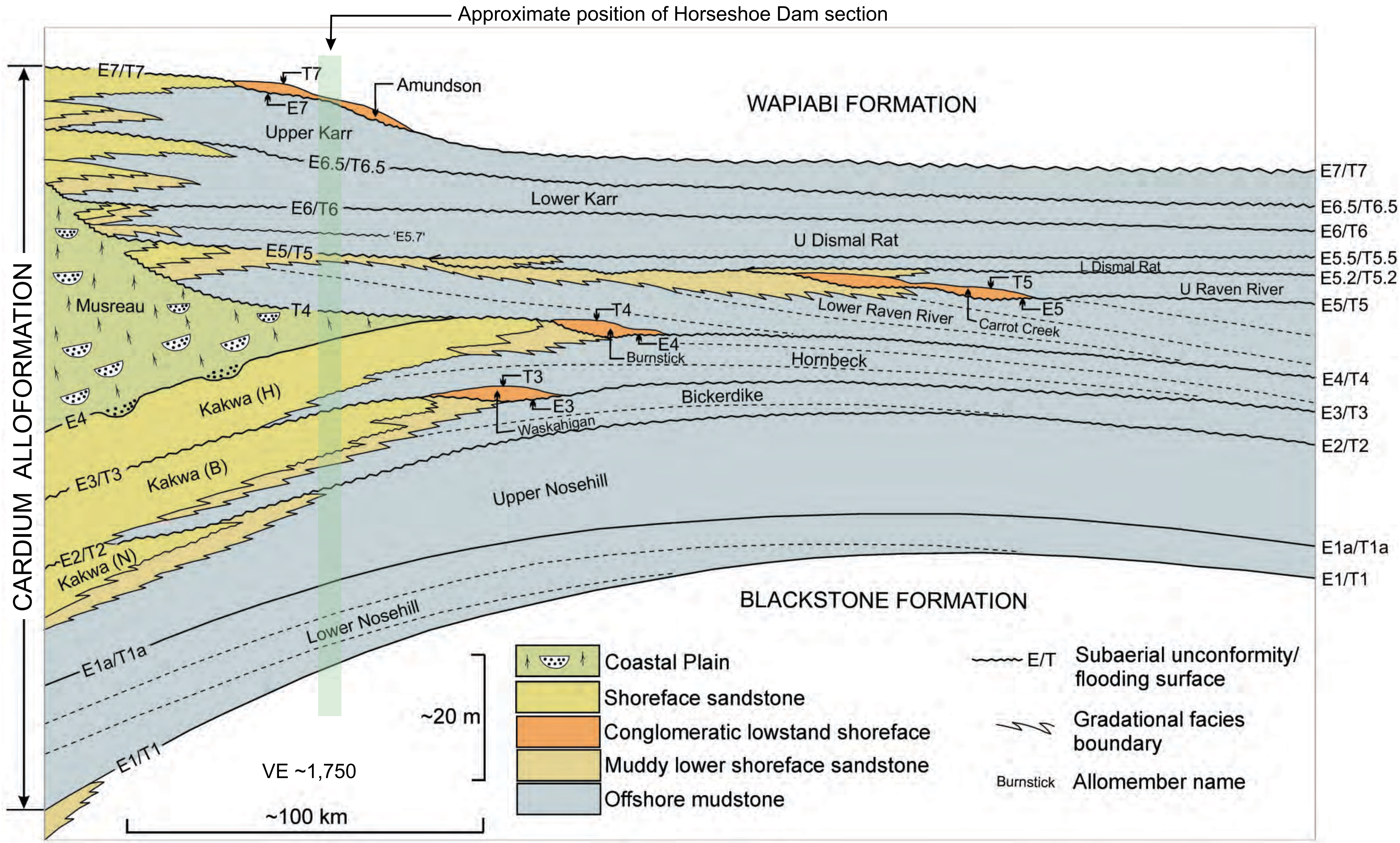

Approximate position of Horseshoe Dam section
WAPIABI FORMATION
BLACKSTONE FORMATION
CARDIUM ALLOFORMATION
E7/T7
T7
E7
Amundson
Upper Karr
E6.5/T6.5
Lower Karr
E6/T6
'E5.7'
U Dismal Rat
E5/T5
L Dismal Rat
T5
E5
U Raven River
Lower Raven River
Carrot Creek
Musreau
T4
E4
Burnstick
Hornbeck
T3
E3
Waskahigan
Bickerdike
E4
Kakwa (H)
E3/T3
Kakwa (B)
Upper Nosehill
E2/T2
Kakwa (N)
Lower Nosehill
E1a/T1a
E1/T1
E7/T7
E6.5/T6.5
E6/T6
E5.5/T5.5
E5.2/T5.2
E5/T5
E4/T4
E3/T3
E2/T2
E1a/T1a
E1/T1
~20 m
VE ~1,750
~100 km
Coastal Plain
Shoreface sandstone
Conglomeratic lowstand shoreface
Muddy lower shoreface sandstone
Offshore mudstone
E/T Subaerial unconformity/ flooding surface
Gradational facies boundary
Burnstick Allomember name

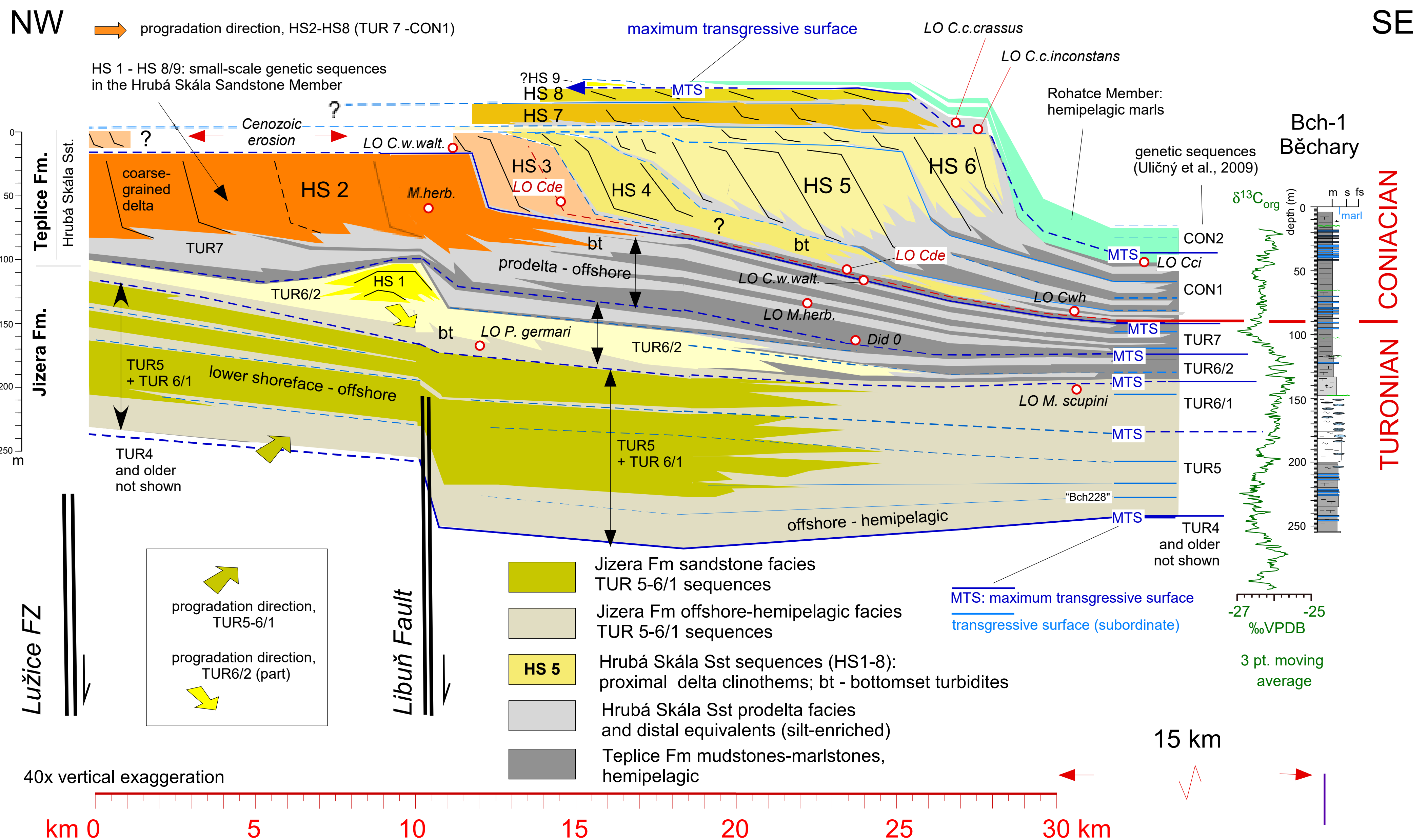

NW
SE
progradation direction, HS2-HS8 (TUR 7 -CON1)
maximum transgressive surface
LO C.c.crassus
LO C.c.inconstans
HS 1 - HS 8/9: small-scale genetic sequences in the Hrubá Skála Sandstone Member
?HS 9
HS 8
HS 7
MTS
Rohatce Member: hemipelagic marls
Cenozoic erosion
LO C.w.walt.
Teplice Fm.
Hrubá Skála Sst.
coarse-grained delta
HS 2
M.herb.
HS 3
LO Cde
HS 4
HS 5
HS 6
genetic sequences (Uličný et al., 2009)
Bch-1 Běchary
CONIACIAN
TURONIAN
TUR7
bt
prodelta - offshore
LO Cde
CON2
LO Cci
CON1
LO C.w.walt.
LO Cwh
LO M.herb.
Jizera Fm.
TUR6/2
HS 1
LO P. germari
Did 0
TUR7
TUR6/2
TUR6/1
TUR5 + TUR 6/1
lower shoreface - offshore
LO M. scupini
TUR4 and older not shown
TUR5 + TUR 6/1
TUR5
"Bch228"
offshore - hemipelagic
TUR4 and older not shown
Lužice FZ
Libuň Fault
progradation direction, TUR5-6/1
progradation direction, TUR6/2 (part)
Jizera Fm sandstone facies TUR 5-6/1 sequences
Jizera Fm offshore-hemipelagic facies TUR 5-6/1 sequences
HS 5
Hrubá Skála Sst sequences (HS1-8): proximal delta clinothems; bt - bottomset turbidites
Hrubá Skála Sst prodelta facies and distal equivalents (silt-enriched)
Teplice Fm mudstones-marlstones, hemipelagic
MTS: maximum transgressive surface
transgressive surface (subordinate)
δ13Corg
depth (m)
m s fs
marl
-27 -25
‰VPDB
3 pt. moving average
15 km
40x vertical exaggeration
km 0
5
10
15
20
25
30 km

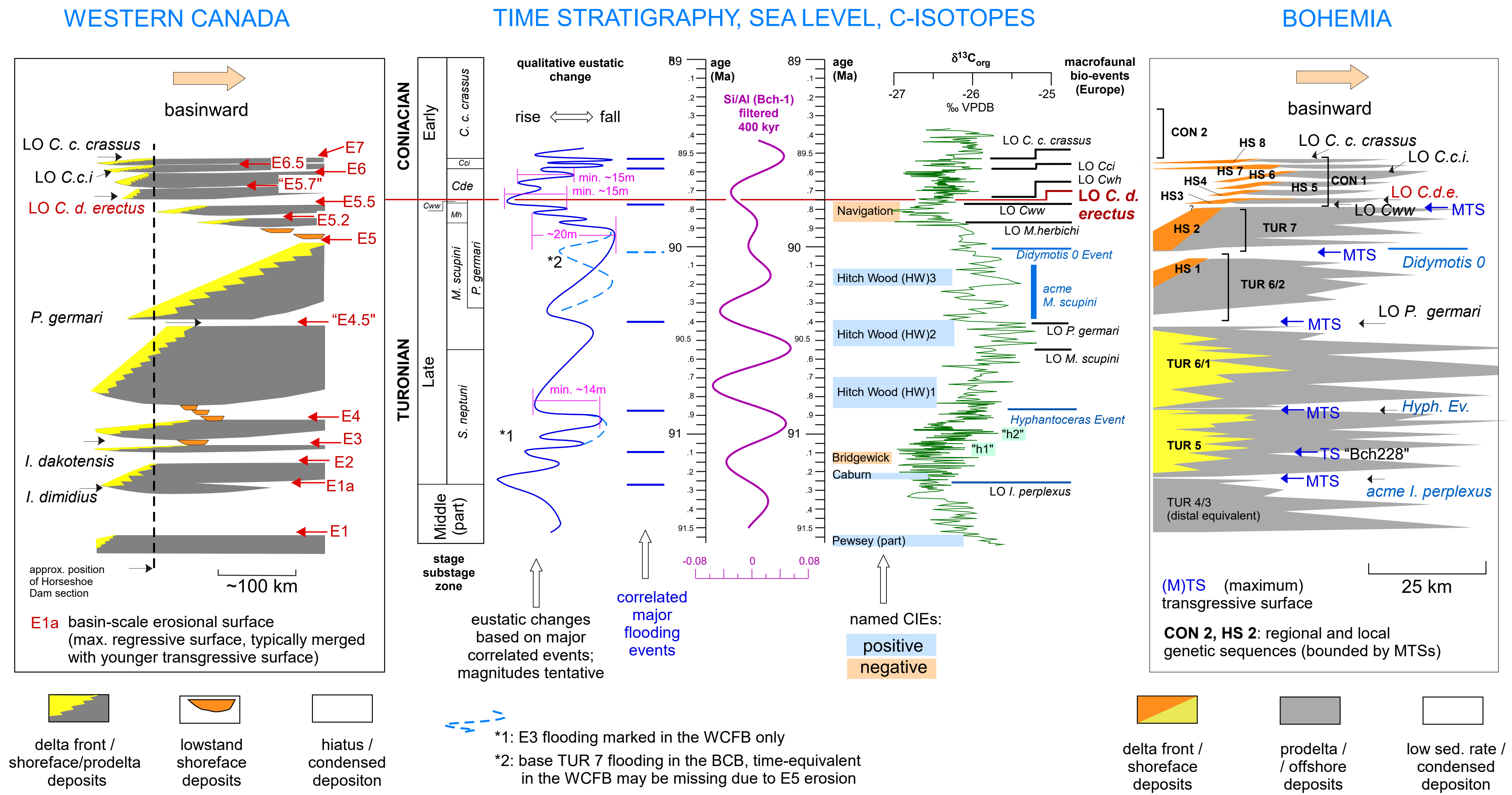

WESTERN CANADA
TIME STRATIGRAPHY, SEA LEVEL, C-ISOTOPES
BOHEMIA
basinward
LO C. c. crassus
LO C.c.i
LO C. d. erectus
P. germari
I. dakotensis
I. dimidius
E7
E6.5
E6
"E5.7"
E5.5
E5.2
E5
"E4.5"
E4
E3
E2
E1a
E1
approx. position of Horseshoe Dam section
~100 km
E1a basin-scale erosional surface (max. regressive surface, typically merged with younger transgressive surface)
CONIACIAN
TURONIAN
Early
Late
Middle (part)
C. c. crassus
Cci
Cde
Cww
Mh
M. scupini
P. germari
S. neptuni
stage substage zone
qualitative eustatic change
rise fall
min. ~15m
min. ~15m
~20m
*2
min. ~14m
*1
eustatic changes based on major correlated events; magnitudes tentative
correlated major flooding events
age (Ma)
Si/Al (Bch-1) filtered 400 kyr
89
89.5
90
90.5
91
91.5
-0.08
0
0.08
δ13Corg
-27
-26
-25
‰ VPDB
macrofaunal bio-events (Europe)
Navigation
Hitch Wood (HW)3
Hitch Wood (HW)2
Hitch Wood (HW)1
"h2"
"h1"
Bridgewick
Caburn
Pewsey (part)
LO C. c. crassus
LO Cci
LO Cwh
LO C. d. erectus
LO Cww
LO M.herbichi
Didymotis 0 Event
acme M. scupini
LO P. germari
LO M. scupini
Hyphantoceras Event
LO I. perplexus
named CIEs:
positive
negative
CON 2
HS 8
HS 7
HS 6
HS4
HS3
HS 5
CON 1
LO C.c.i.
LO C.d.e.
LO Cww
MTS
HS 2
TUR 7
HS 1
TUR 6/2
Didymotis 0
LO P. germari
TUR 6/1
Hyph. Ev.
TUR 5
TS "Bch228"
acme I. perplexus
TUR 4/3 (distal equivalent)
25 km
(M)TS (maximum) transgressive surface
CON 2, HS 2: regional and local genetic sequences (bounded by MTSs)
delta front / shoreface/prodelta deposits
lowstand shoreface deposits
hiatus / condensed depositon
*1: E3 flooding marked in the WCFB only
*2: base TUR 7 flooding in the BCB, time-equivalent in the WCFB may be missing due to E5 erosion
delta front / shoreface deposits
prodelta / offshore deposits
low sed. rate / condensed depositon